Kinetic Shapes: Analysis, Verification, and Applications

Ismet Handžić★ and Kyle B. Reed†

Department of Mechanical Engineering
University of South Florida
Tampa, Florida 33620
Email: ★ihandzic@mail.usf.edu, †kylereed@mail.usf.edu

A circular shape placed on an incline will roll; similarly, an irregularly shaped object, such as the Archimedean spiral, will roll on a flat surface when a force is applied to its axle. This rolling is dependent on the specific shape and the applied force (magnitude and location). In this paper, we derive formulas that define the behavior of irregular 2D and 3D shapes on a flat plane when a weight is applied to the shape's axle. These kinetic shape (KS) formulas also define and predict shapes that exert given ground reaction forces when a known weight is applied at the axle rotation point. Three 2D KS design examples are physically verified statically with good correlation to predicted values. Motion simulations of unrestrained 2D KS yielded expected results in shape dynamics and self-stabilization. We also put forth practical application ideas and research for 2D and 3D KS such as in robotics and gait rehabilitation.

Nomenclature
Two-dimensional Shape
θ Angle around shape axle
$R(\theta)$ Shape radius
$\psi(\theta)$ Angle relating shape tangent to vector and applied weight to radial force
$F_v(\theta)$ Weight applied at axle perpendicular to ground
$F_r(\theta)$ Radial ground reaction force parallel to ground
$L(\theta)$ Horizontal distance between applied weight vector to ground contact point
$H(\theta)$ Vertical distance between shape axle and ground

Three-dimensional Shape
θ, ϕ Elevation and azimuth angle around shape axle
$R_r(\theta,\phi)$ Shape radius in the radial plane
$R_t(\theta,\phi)$ Shape radius in the tangential plane
$F_v(\theta,\phi)$ Weight applied orthogonal to ground
$F_r(\theta,\phi)$ Radial ground reaction force (RGRF) of shape parallel to ground
$F_t(\theta,\phi)$ Tangential ground reaction force (TGRF) of shape parallel to ground

1 Introduction
It is easily demonstrated that a perfectly circular shape does not roll on a flat surface, but only rolls when placed onto a decline. By straightforward dynamic analysis of a circular shape, it is obvious that when placed on a decline the sum of moments does not equal zero, hence the shape will roll. It can also be demonstrated that a smooth two-dimensional polar shape with a non-constant radius will roll

on a flat surface around the instantaneous point of contact. It will roll toward the decreasing radius with respect to angle when a vertical force is applied to its axle. Both of these situations create the same instantaneous dynamic rolling effect, illustrated in Fig. 1.

The rolling of a circular wheel is definitely not novel, but the rolling of an irregularly curved shape, such as a spiral rolling on a flat surface, is useful and has not received much research attention. In this paper, we show how to derive two- and three-dimensional shapes that, when placed on a flat plane and loaded with a known weight at the axle point, will produce a desired ground reaction force parallel to the flat plane. This derived shape with known force parameters can in turn be used in static and dynamic applications some of which include, but are not limited to, self-stabilization, material hardness testing, robotic control, and gait manipulation.

This paper defines and validates applications of two- and three-dimensional shapes that have a predictable kinetic and kinematic profile across their perimeter surface. Due to their predictive kinetic parameter, we will call these shapes *kinetic shapes* (KS).

2 Background
Two centuries B.C., astronomer and mathematician Conon of Samos was the first to study conic sections, which are curves created by the intersections of cones. His work greatly inspired a colleague, Archimedes, to further study a special two dimensional curve now known as the Archimedean spiral (AS) [1]. The AS is given by Eqn. (1),

$$R(\theta) = a + b\theta, \tag{1}$$

where a and b are arbitrary spiral constants. While there are many variations of such a curve (e.g., Logarithmic Spiral, Cortes Spiral, etc.), the AS is defined in polar coordinates as a curve that increases at a steady rate in radius as the angle increases. This shape is particularly interesting in its
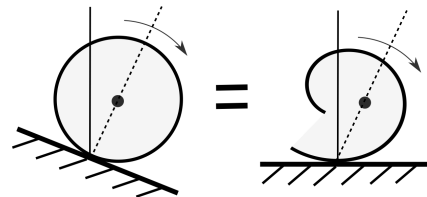

Fig. 1. A circular wheel on a decline and a shape with a negatively changing radius are instantaneously equivalent in rolling dynamics.

physical form, in that it rolls by itself on a flat surface and closely mimics a circular wheel rolling down a hill. While the physical form of the AS is applicable in many disciplines, such as fluid compression [2] or microbiology [3], it is found to be attractive to mechanical designs where passive rolling or force redirection is desired.

Such a design is the Gait Enhancing Mobile Shoe (GEMS) [4, 5] for gait rehabilitation of individuals with neurological disorders such as stroke. The GEMS mimics a split-belt treadmill (a treadmill with two independently controlled treads) by pushing the individual's foot backward as they step onto the shoe with AS-shaped wheels. As the user applies their weight onto the spiral wheels, the wheels react by rolling horizontally. This method is completely passive in that it does not utilize any energized motors or actuators, but only uses the person's weight to create motion. Unlike a split-belt treadmill, the GEMS is portable and can apply rehabilitative motions for a longer amount of time. This two dimensional rolling motion is essentially created by the changing of the radius in a rounded shape.

Similarly, a deformable crawling and jumping soft robot [6] can use this rolling principle where the initial circular shape is mechanically deformed, which causes it to roll on a flat surface and it can even roll up a slope. This circular robot progresses forward by shortening and lengthening internal chords that are attached to an outside rim. As the rim is systematically deformed by the chords, the robot rolls forward or backward. This crawling robot used the same principle to construct a sphere that can roll [6]. This study of a crawling and jumping deformable soft robot only addresses the hardware, software, and motion energy analysis, but is missing an explanation of the rolling kinetics and an analytical description of the motion.

A static version of a spiral shape is used in rock climbing equipment. The safety equipment known as a spring-loaded camming device (SLCD) [7] is commonly used by rock climbers to secure their rope into a rock crack while climbing. The SLCD utilizes two freely spinning spiral-shaped cams facing opposite directions. When the climber falls and applies a sudden force between the spiral cams and the rock surface, the cams are pushed outwards increasing friction between the cams and rock surface and providing enough force to resist the falling climber. This static force redirection is similar, but opposite, to the previously described GEMS and rolling robot in that it directs horizontally applied force into a perpendicular force. While this climbing innovation has been on the market for decades, the authors are not aware of any significant analysis/research that has been published regarding the variation of forces along the cam perimeter and optimization of its logarithmic spiral shape.

Spiral-shaped wheels have a resemblance to objects with an eccentric rotation point, such as cams [8, 9]. Research on cam design focuses on the transfer of kinematics of two or more entities, generally rotary motion (the cam) into linear motion (the follower). While research on camming generally focuses on kinematics and tribology, it does not have free or forced rolling dynamics or force redirection of continuous irregular shapes.

The study of belt drives [10] and gearing [11] generally focuses on torque, rotational velocities, and normal forces between gear tooth surfaces. This includes the kinematics of circular and non-circular (elliptical) belt pulleys [12] and gears [13], and the kinematics of rack and pinion type of mechanisms [14]. Again, little is found in this area for free rolling and force redirection of irregular shapes. One related study derived a square wheel with matching roads (a type of rack and pinion) [15] that showed some insight into irregular shape rolling kinematics, but kinetics and static equilibrium of these shapes are not addressed.

One study considered the geometry of 2D circular, non-circular, and logarithmic shape rolling [16]. However, it did not consider any kinetics and strictly focused on the traces of curves (roulettes) created when rolling over various surfaces.

Spiral patterns are also possible in 3D, such as a rhumb line (loxodrome). We include helix type spirals in our definition of 3D spirals, which have no change in radius, only in the depth dimension. No literature could be found that defines the kinetic or kinematic behavior of such shapes (or curves) during free or forced rolling dynamics. However, such research is needed for gait correction and rehabilitation.

Roll over shapes (ROS) are foot rocker shapes that the foot rolls over when completing the stance phase during the gait cycle. ROS have enormous effects in gait kinematics, kinetics, and balance [17], and ROS are important in prosthetic design [18, 19, 20]. However, current gait studies have not been able to analytically predict the behavior of ROS. Hanson et al. [20] state *"A better understanding [of ROS] could be used to develop improved prostheses, perhaps improving balance and balance confidence, and reducing the occurrence of falling in lower limb prosthesis users"*. A significant issue in lower limb prosthetic designs are the forces exerted by the prosthetic onto the user's stump. These forces can be manipulated or even diminished if the ROS is modified properly [21]. Besides prosthetic design, orthotic therapy and gait rehabilitation using specially-designed shoe soles can benefit patients of diseases such as cerebral palsy, parkinson's, and stroke [22], and increase muscle activity of selected foot muscles [23].

ROS also play a crucial role in the design of passive dynamic walkers (PDW), which can be used to predict normal and pathological human gait [24]. A PDW (2D or 3D) mimics human gait by walking down an incline solely due to gravity, hence they are completely passive. Through design trials, McGeer indicates a most effective foot rocker radius to be 1/3 of total leg length [25], exactly matching the most efficient human ROS radius [26]. Although PDW ROS are a key component to the dynamics and stability of PDWs, currently the authors are not aware of any literature that specifically specifies the size or shape of PDW ROS.

3 Two-Dimensional Kinetic Shape

In this section we derive, validate, and present design examples of two-dimensional kinetic shapes.

3.1 Mathematical Model Derivation

A curved and continuous arbitrarily 2D shape that is pressed onto a flat plane at its axle point tends to rotate towards the decreasing radius. This rotation is because the applied weight is not vertically in line with the point of ground contact, which creates unmatched moment couples with the radial ground reaction force (RGRF). Hence, the shape is not in static equilibrium and will roll.

However, if the rolling motion of this shape is restrained by a horizontal force at the axle point so that the shape is in static equilibrium, the sum of all forces and moments must equal zero (Fig. 2(a)). For this to happen, the moment couple created by the RGRF (friction) and the equal and opposite restraining force has to be equal to the moment couple created by the applied weight and the equal and opposite vertical ground reaction force. Because the shape varies in radius, the RGRF component pushing away from the axis, $F_r(\theta)$, must vary as well.

It is assumed that the friction force between the ground and the shape is large enough for the shape not to slip. It is also assumed that there is no deformation of the shape or ground. This analysis is also only valid when the applied force at the shape axle is much greater than the combined gravitational forces applied at the center of mass of the shape or if the center of mass coincides with the shape axle.

We will derive a general formulation to create a shape that will generate a desired RGRF given a known applied weight. We begin by adding the two moment couples acting on a general 2D shape under static equilibrium

$$\sum M_z = F_v(\theta)L(\theta) - F_r(\theta)H(\theta) = 0 \qquad (2)$$

where $L(\theta)$ and $H(\theta)$ are shown in Fig. 2(a), and defined as

$$H(\theta) = R(\theta)\sin(\psi(\theta)), \qquad (3)$$

$$L(\theta) = R(\theta)\cos(\psi(\theta)), \qquad (4)$$

and $\psi(\theta)$ is defined in Fig. 2(a). Substitution of Eqn. (3) and (4) into the statics equilibrium Eqn. (2) yields

$$F_v(\theta)[R(\theta)\cos(\varphi(\theta))] = F_r(\theta)[R(\theta)\sin(\varphi(\theta))]. \qquad (5)$$

Dividing out $R(\theta)$ and applying appropriate trigonometric identities results in

$$\psi(\theta) = \tan^{-1}\left(\frac{F_v(\theta)}{F_r(\theta)}\right). \qquad (6)$$

Eqn. (6) defines the angle $\psi(\theta)$ along the perimeter of the shape. $\psi(\theta)$ relates the weight applied at the shape axle and the RGRF at ground contact.

$\psi(\theta)$ can also be defined as the angle at the point of ground contact between the ground vector (shape tangent), $dR/d\theta$, and the radial vector (axle to ground contact point), $R(\theta)$, as shown in Fig. 2(b) [27]. This relation is defined as

$$\psi(\theta) = \tan^{-1}\left(\frac{R(\theta)}{dR/d\theta}\right). \qquad (7)$$

It is now apparent that we can equate and reorder Eqns. (6) and (7) to form a first order ordinary differential equation.
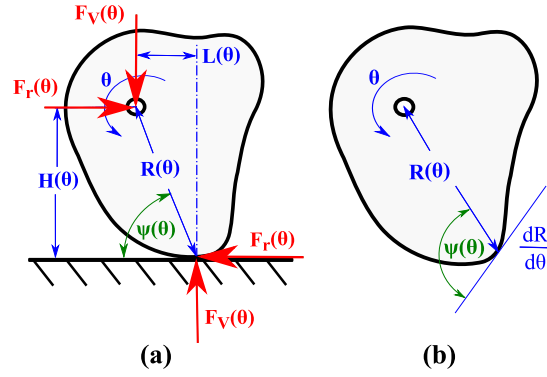

Fig. 2. (a) Static equilibrium of a kinetic shape. (b) Kinetic shape geometric parameters.

$$\frac{dR}{d\theta} = \frac{R(\theta)F_r(\theta)}{F_v(\theta)} \qquad (8)$$

Eqn. (8) can be solved using the method of separation of variables by first rearranging,

$$\left(\frac{1}{R(\theta)}\right)dR = \left(\frac{F_r(\theta)}{F_v(\theta)}\right)d\theta, \qquad (9)$$

then integrating both sides of the equation to solve for the shape radius.

$$R(\theta) = \exp\left[\int\frac{F_r(\theta)}{F_v(\theta)}d\theta + \text{Constant}\right] \qquad (10)$$

The integration constant is dependent on the initial radius of the shape. Eqn. (10) will derive a 2D *kinetic shape (KS)* that produces a RGRF, $F_r(\theta)$, when a load perpendicular to the ground at axle point, $F_v(\theta)$, is applied. Section 3.3 shows how Eqn. (10) is used to design a shape and experimentally validates several force profiles.

The derived shape can be checked to determine if it produces the desired reaction forces when loaded by taking the obtained shape $R(\theta)$ and finding $\psi(\theta)$ in Eqn. (7), then inputting it back into Eqn. (6). The resulting forces should match the initial input forces. This also enables one to find the kinetic profile of any irregular curved 2D shape.

The 2D KS equation, Eqn. (10), yields a unitless radius value. This indicates that it only depends on the force ratio rather than the size of the shape. Thus, when loaded with a fixed weight, the same KS with different scaling factors will produce the same RGRF. For example, a KS for a constant 800 N weight and constant 200 N RGRF input will be the exact same as a KS for a constant 4 mN vertical and constant 1 mN RGRF input regardless of its scaled dimensions.

3.2 Physical Verification Experiment

The kinetic shape can be verified with the simple setup shown in Fig. 3. The weight is applied to the shape axle and the reaction forces exerted by the shape axle are both measured with a load cell sensor (Omega LC703) placed in line with the forces. To prevent the KS from slipping, two-sided course grade sandpaper was placed at ground contact. As the applied weight was gradually loaded, the RGRF increased as well.

The tested KS were loaded at $\pi/6$ rads intervals from zero to 2π rads. Some perimeter points, such as the lowest
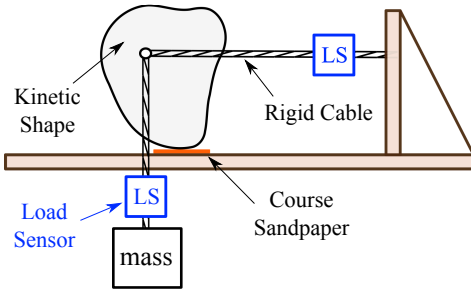
Fig. 3.   Schematic of test structure for 2D kinetic shapes

radii on a spiral shape, were omitted because the ground contact could not reach that particular perimeter point (i.e., Fig. 4(a) at 0 rads), however this usually was only one point.

The reaction load for each perimeter point was recorded with a mass of 7.9 kg to 18.0 kg at four even intervals applied to the shape axle. The mean and standard deviation for each point was calculated in terms of percent force transfer ($100 *$ $F_r(\theta)/F_r(\theta)$), which was then multiplied by 800 N.

Three 2D KS examples were chosen for verification and were laser cut from tough 0.25 in (0.64 cm) thick Acetal Resin (Delrin®) plastic. The laser cutter used to cut test shapes was a 60 Watt Universal Laser System® VLS4.60.

3.3   Model Result Design Examples

To demonstrate example KS designs using Eqn. (10), three different desired force functions with constant applied weight were chosen: constant, sinusoidal with an offset, and Fourier series expanded non-smooth RGRF function. Each derived KS assumed a constant vertical force of 800 N. The magnitude of these force functions were chosen for the convenience of experimentation. Although the analysis can be expanded to KS that revolve more than once, we focus on shapes that range from zero to 2π rads. It is important to note that if the 2D shape is to be continuous around one revolution, Eqn. (11) must be satisfied.

$$\int_0^{2\pi} F_r(\theta)\,d\theta = 0 \qquad (11)$$

3.3.1   2D Shape 1: Constant RGRF

To introduce the KS design concept, we start with a shape defined by a constant force function and a constant applied weight function. Eqns. (12) and (13) describe the input functions used to derive the first 2D KS. The KS was started with an initial shape radius of 2.5 in (6.35 cm) and ends with a 5.46 in (13.86 cm) radius.

$$F_v(\theta) = 800\,N \qquad (12)$$

$$F_r(\theta) = 100\,N \qquad (13)$$

With these forces and initial radius, Eqn. (10) becomes

$$R(\theta) = \exp\left[\frac{100}{800}\,\theta + \ln(2.5)\right]_{\theta=0}^{\theta=2\pi}. \qquad (14)$$

As an 800 N force is applied at the shape axle, the shape will react with a 100 N force regardless of the rotation angle.   As seen in Fig. 4(a), the gradual and

slight exponential increase in shape radius, *dR/d*θ, statically produces a constant force at any perimeter point around the shape, creating a spiral KS. Note that the units, and thus the scaled size, are irrelevant and this KS would behave the same if scaled up or down.

As seen in Fig. 4(a), the physical measurements are in good agreement with theoretical values. There are some variations; however, these can be accounted for by shape surface and test setup imperfections. Although the force profile standard deviation is not always within predicted theoretical range, the trend is relatively constant.

3.3.2   2D Shape 2: Sinusoidal RGRF

A KS can also be derived using a more complicated sinusoidal force function with a constant offset. Eqns. (15) and (16) describe the input functions that define this 2D KS.

$$F_v(\theta) = 800\,N \qquad (15)$$

$$F_r(\theta) = 100\sin(\theta) + 100\,N \qquad (16)$$

With these forces, Eqn. (10) then becomes

$$R(\theta) = \exp\left[\frac{1}{8}(\theta - \cos(\theta)) + \ln(1.75)\right]_{\theta=0}^{\theta=2\pi}. \qquad (17)$$

Unlike in the previous example that produces a constant RGRF, this shape creates a varying sinusoidal force throughout the rotation. In this example design it is clear that the reaction force is dependent on $dR/d\theta$ of the shape. As the sinusoidal force reaches a maximum at $\pi/2$, $dR/d\theta$ is steepest and produces the highest RGRF. Likewise, as the input force reaches a minimum of zero at $3\pi/2$, $dR/d\theta$ is zero as well. At $3\pi/2$ the KS instantaneously behaves as a circular wheel would, and, like a circular wheel, it does not produce a RGRF when vertically loaded at its axle.

The KS assumes a spiral shape with a starting radius of 1.75 in (4.44 cm) and a final radius of 3.82 in (9.70 cm). The shape again resembles a spiral due to the fact that the sum of force around the shape perimeter is non-zero as defined by Eqn. (11). The physically measured force profile for this 2D KS, shown in Fig. 4(b), was slightly higher than predicted, however the sinusoidal trend was in good agreement.

3.3.3   2D Shape 3: Fourier Expanded Piecewise Force

It is clear now that a KS can be designed with any input force function. We expand our analysis to a piecewise force function that has been expanded using ten Fourier series terms to demonstrate that nearly any force profile can be created. This piecewise force function is defined as

$$F_v(\theta) = 800\,N \qquad (18)$$

$$F_r(\theta) = \begin{cases} 200\,N, & 0 \le \theta \le 3.8 \\ 4380 - 1100\,\theta\,N, & 3.8 < \theta < 4.3 \\ -350\,N, & 4.3 \le \theta < 2\pi \end{cases} \qquad (19)$$

Note that this time the RGRF function crosses zero at 4.1 rads (Fig. 4(c)). At exactly this point, the shape produces no force and the radius starts to decrease in order to produce a negative force. This shape does not form a spiral, but is
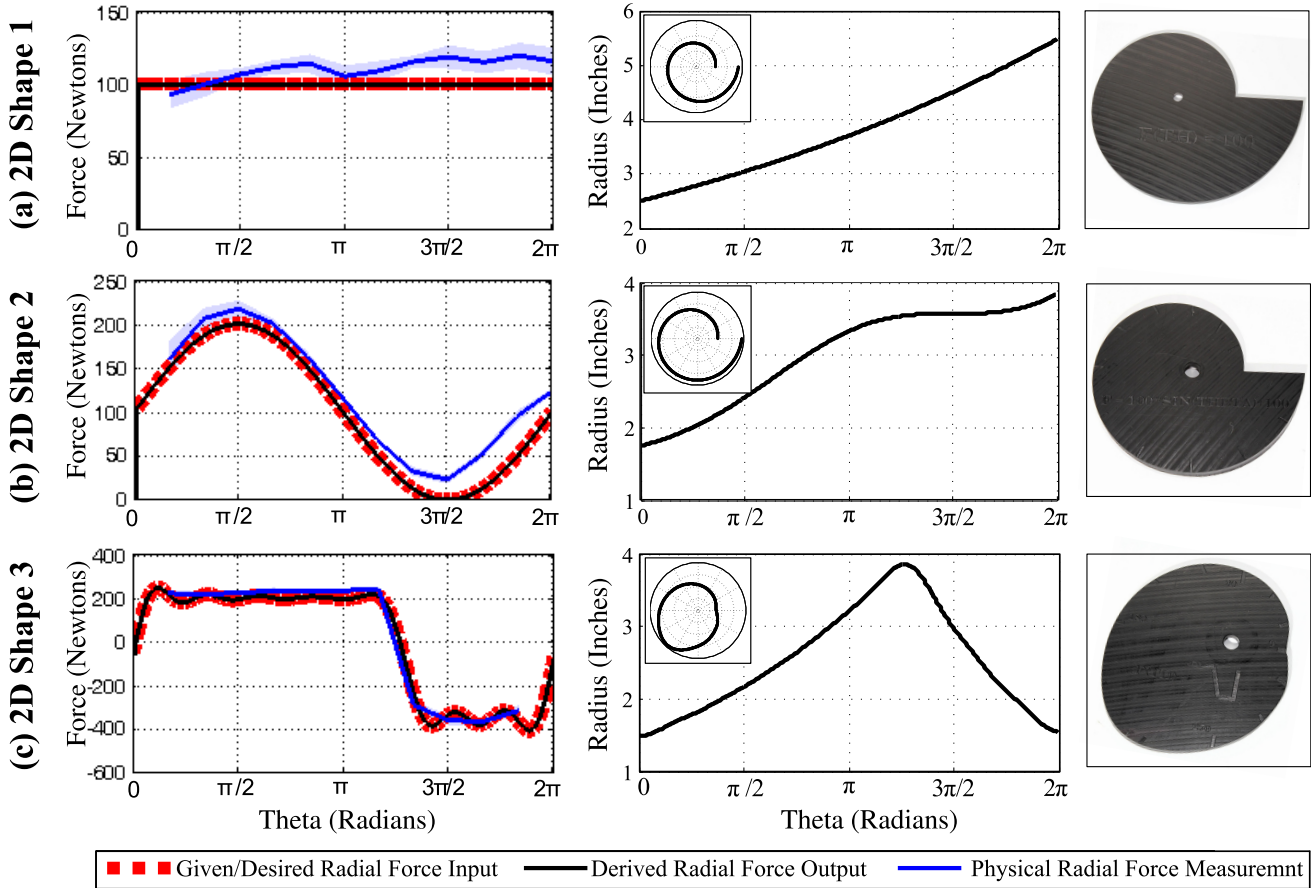
(a) 2D Shape 1

(b) 2D Shape 2

(c) 2D Shape 3

■ ■ ■ Given/Desired Radial Force Input   ——— Derived Radial Force Output   ——— Physical Radial Force Measuremnt

Fig. 4. **(a)** 2D Shape 1 forms a spiral with a steadily increasing radius as it is defined by a constant vertical force input and a constant RGRF output all around the shape. **(b)** 2D Shape 2 forms a monotonically increasing radius spiral, however when a constant weight is applied, it reacts with a sinusoidal RGRF around its perimeter. **(c)** 2D Shape 3 forms a continuous shape because, when a constant weight input is applied, it initially reacts with a positive reaction force and then switches directions to form a negative RGRF. All physical measurements are in good agreement.

continuous around its perimeter, starting and ending at the same radius, hence Eqn. (11) is satisfied.

Measurements on the physical shape verified the predicted values. As seen in Fig. 4*(b)*, physical data falls well within theoretical values. Note that the standard deviation of measurements increases where the force profile fluctuates the most.

3.4 Shape Dynamics

A restrained 2D KS is able to statically produce desired reaction forces; however we can utilize an unrestrained kinetic shape to exert a known force around its perimeter over time in a dynamic setting. In other words, a KS can be obtained to exert a predicted dynamic force onto an object or itself creating a predicted dynamic response.

One application of a kinetic shape in a dynamic setting is to displace a flat plate on the ground. We assume a no-slip condition between the KS and the flat plate, and no friction between the flat plate and ground. Also, the shape axle is constrained to only move along the vertical direction as shown in Fig. 5.

As a vertical force is applied to the KS, RGRF push the flat plate in the horizontal direction, thus changing its velocity. To illustrate this concept, we simulated the
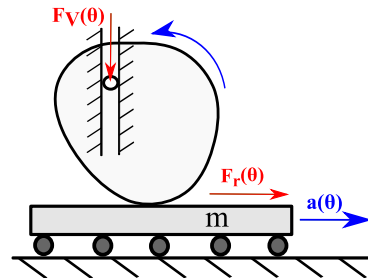

Fig. 5. A flat plate with a known mass is dispensed with a predicted linear acceleration.

sinusoidal KS that weighs 0.01 kg (0.1 N) (Fig. 4(b)) being pushed vertically at its axle with 8.0 N force onto a flat plate weighing 0.5 kg (4.9 N). The shape mass with respect to the dispensed plate is considered negligible. All dynamic behavior was analyzed with SolidWorks Motion Analysis®.

Fig. 6 shows the plate velocity and shape rotation position versus time. The magnitude of the applied vertical force only affects the simulation time. Because the shape was not continuous all around, setup dynamics were recorded from 2π to 1.7 rads, rolling from the greatest radius at 2π to the lowest radius.

Referring back to Fig. 4(b), this velocity profile perfectly shows the effect of changing the sinusoidal output
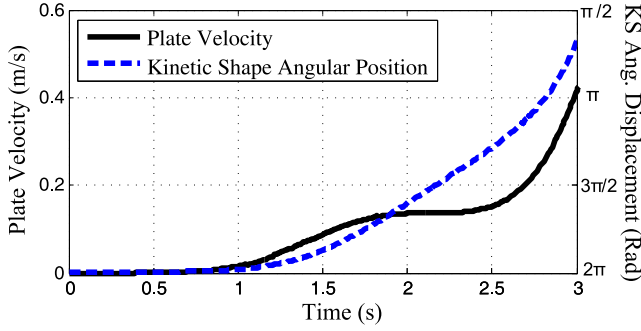
Fig. 6. Dynamic interaction of 2D Shape 2 onto a flat plate (0.5 kg). The applied weight is constant as the kinetic shape pushes the plate.

force around the shape. Adhering to the basic principle dynamic of Newton's second law, as the RGRF decreases to zero, so does the acceleration of the moving plate, creating a plateau in plate velocity at $3\pi/2$. Thereafter, the pushing force increases dramatically and so does the plate velocity.

Although this simulation setup and results are insightful of pushed plate dynamics, it can be relatively viewed as regular over-ground rolling of the KS, where the shape moves over a stationary surface. However, in over-ground shape rolling, the changing moment of inertia about ground contact factors into the rolling dynamics, which can obfuscate this example. If the weight applied at shape axle is much larger then the weight of the shape itself, shape inertial forces can be neglected. We leave this to future work.

3.5 Mechanical Self-Stabilization

Dynamic self-stabilization is an interesting mechanical aspect of an unrestrained KS. A system that is able to self-stabilize will correct its state to a stable value when perturbed by an external force or when started at any other state. When an unrestrained and rolling KS RGRF profile switches signs, crossing the zero axis, it creates a stable point. Once loaded, the shape will roll around its perimeter, eventually settling onto this zero stable point due to non-conservative damping forces such as friction.

This behavior can be observed in Fig. 7, where the KS RGRF is described by a simple sinusoid switching force sign at 0 and π rads. In a virtual simulation with SolidWorks Motion Analysis®, this shape is pushed down with a constant weight (50 N) that is significantly larger then
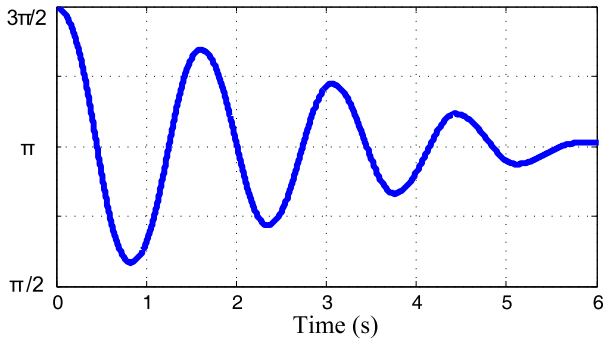

Fig. 7. When disturbed or placed at an unstable position, a two-dimensional kinetic shape settles at its equilibrium point.

the shape weight (0.1 kg; 1 N) starting at $3\pi/2$ rads after which it oscillates and comes to a halt at π rads. While the behavior is consistent, the settling time, of course, is dependent on the applied weight, shape mass (and/or plate mass), and non-conservative forces. It is stressed that shape inertia becomes negligible if the applied weight is much larger then the shape weight. This concept can be utilized in any mechanical structure where the stable position of the structure is important after disruptive forces are applied.

4 Three-Dimensional Kinetic Shape

We expand our analysis into the third dimension by deriving and analyzing a 3D KS. The behavior of a 3D KS can sometimes become hard to visualize. While a 2D KS produces only one RGRF that pushes radially away from the shape's axle, a 3D KS can theoretically produce two force components: the same RGRF pushing away from the axle point and a tangential ground reaction force (TGRF) pushing around the vector of weight application that is orthogonal to the ground plane.

To visualize the TGRF, imagine a cylinder sitting on a flat plane (e.g., a cup on a table) as shown in Fig. 8. If the cylinder is tipped over, the ground experiences only a RGRF to keep it from slipping. However, if the cylinder's sides are not uniform in length around its perimeter, such as in a helix curve, the tipped helix will tend to push and roll around the vertical axis which runs through the center of mass and is perpendicular to ground. This rolling motion is caused by the TGRF acting on the cylinder's rim. This TGRF can also be generated if a 2D KS is wrapped around a vertical axis with a non-constant radius.

4.1 Mathematical Model Derivation

We seek to derive a set of equations that allows us to construct a shape that produces a known RGRF and TGRF when vertically loaded. Similar methods and assumptions utilized to derive a 2D KS are used to produce an analytical model of a 3D KS.

We begin by examining a 3D shape/curve in static equilibrium, shown in Fig. 9. The summation of all moment couples in the radial plane and about the vertical vector yields the following equations:

$$\sum M_r = F_v(\theta,\phi)R(\theta,\phi)\cos(\psi) \ldots \qquad (20)$$
$$-F_r(\theta,\phi)R(\theta,\phi)\sin(\psi) = 0$$

$$\sum M_v = [F_t(\theta,\phi)\cos(\phi)]\,(R(\theta,\phi)\cos(\psi)\cos(\phi)) \ldots \quad (21)$$
$$-[F_r(\theta,\phi)\cos(\phi)]\,(R(\theta,\phi)\cos(\psi)\sin(\phi)) = 0\,.$$
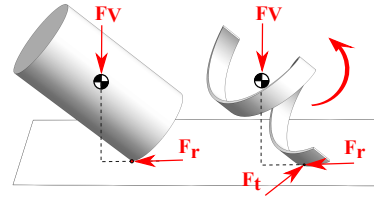

Fig. 8. While a cylinder only produces a RGRF force to keep it from slipping, a helix curve produces an additional TGRF for sideways rolling, as illustrated in this figure.

These kinetic equilibrium equations are simplified, rearranged and related to the geometric parameters shown in Fig. 10, following a similar derivation as shown in Sec. 3.1.

$$\tan(\psi) = \frac{F_r(\theta,\phi)}{F_v(\theta,\phi)} = \frac{R(\theta,\phi)}{dR/d\theta} \qquad (22)$$

$$\tan(\phi) = \frac{F_t(\theta,\phi)}{F_r(\theta,\phi)} = \frac{dR/d\phi}{R(\theta,\phi)} \qquad (23)$$

Angle ψ again relates forces in the radial plane while also relating the radial vector to the ground plane. Angle ϕ relates the TGRF to the RGRF while also relating the geometric parameters shown in Fig. 10.

After rearranging terms, we are left with two first order ordinary differential equations.

$$\left(\frac{1}{R(\theta,\phi)}\right)dR = \left(\frac{F_r(\theta,\phi)}{F_v,\theta,\phi)}\right)d\theta \qquad (24)$$

$$\left(\frac{1}{R(\theta,\phi)}\right)dR = \left(\frac{F_t(\theta,\phi)}{F_r,\theta,\phi)}\right)d\phi \qquad (25)$$

By the method of separation of variables, $R(\theta,\phi)$ yields

$$R_r(\theta,\phi) = \exp\left[\int \frac{F_r(\theta,\phi)}{F_v(\theta,\phi)}\,d\theta + \text{Constant}\right] \qquad (26)$$

$$R_t(\theta,\phi) = \exp\left[\int \frac{F_t(\theta,\phi)}{F_r(\theta,\phi)}\,d\phi + \text{Constant}\right] \qquad (27)$$

Eqns. (26) and (27) jointly describe a 3D KS that relates an applied weight, RGRF, and TGRF. These radius equations describe the shape in the radial and tangential direction, respectively. As before, a radial force is produced by the change in radius with elevation angle, while TGRF is produced by a change in azimuth angle.

In the absence of a TGRF, Eqn. (26) is Eqn. (10), and in the absence of a TGRF forms the same 2D shape. This is made clear when examining Eqn. (27), where as the force ratio diminishes, the radius does not change in the tangential direction. Also, as the force ratio increases, the shape increases exponentially in the tangential direction radius.
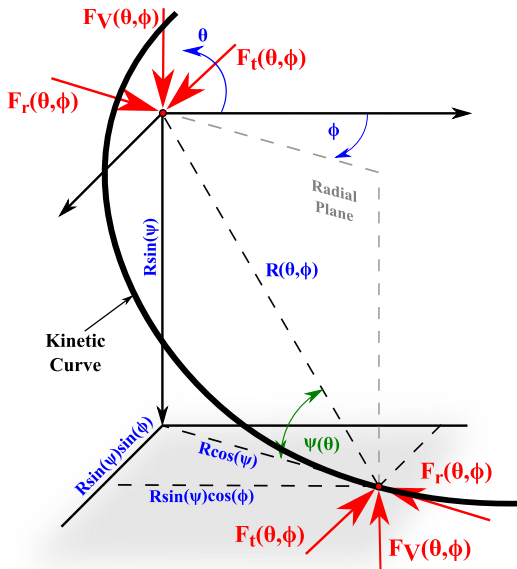

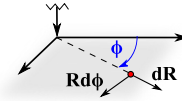Fig. 9.   Free body force diagram of a 3D kinetic shape

Fig. 10.   Geometric parameters at 3D shape ground contact

4.2   Model Result Example

To illustrate the 3D KS represented by Eqns. (26) and (27), we derive a shape, which when loaded with a known weight will produce a specified radial and TGRF. The following force functions define this KS.

$$F_v(\theta,\phi) = 800\,\text{N} \qquad (28)$$

$$F_r(\theta,\phi) = 60\,\theta\,\text{N} \qquad (29)$$

$$F_t(\theta,\phi) = 100\sin(\phi) + 200\,\text{N} \qquad (30)$$

The KS force function along with the integration path (i.e., shape rotation path) in the radial and tangential direction are shown in Fig. 11(a), while the derived shape along with the surface and curve rendering is displayed in Fig. 11(b).

Single and subsequent integration paths can form a KS curve and surface, respectively, however a KS *surface* often cannot statically or dynamically behave as predicted when weight is applied at the axle point due to the interaction between integration paths. Invalid surfaces arise when integration paths that form the surface are not continuously accessible to the ground plane. In many cases, kinetically defined surfaces can be found in which all integration paths are possible, enabling the surface to exert force onto a ground plane.

While we do not present the physical verification of this 3D KS, static analysis of this shape could be done using a force plate, similar to what was done in the 2D case. Dynamic analysis could be done by placing the 3D shape on a simultaneously rotating and radially extending disc surface.

5   Design Applications and Ideas

2D and 3D static and dynamic KS can be utilized in many mechanical methods and designs. In this section a few applications are analyzed and discussed.

5.1   Load Testing Equipment

The static application of a 2D KS can be desirable in surface hardness/properties testing. Consider a surface microindentation hardness testing device/method such as Rockwell, Brinell, or Vickers hardness test. A 2D KS can be derived such that the examiner utilizes only one applied weight while only having to rotate the kinetic shape in order to get a variable load applied onto the surface micro indentation device.

5.2   Variable Dynamic Output for Mobile Robotics

It was shown that a 2D KS can be derived that creates a predictable linear kinematics profile of a pushed plate. This concept can be useful in the realm of mobile robotics, where the velocity profile of robot linkages or any robot movement is crucial. This method offers a mechanical alternative to electronic robot dynamics manipulation and trajectory control. While the 2D KS can produce a predictable kinetic and kinematic linear movement, a 3D KS can be used to produce expected rotary motion.
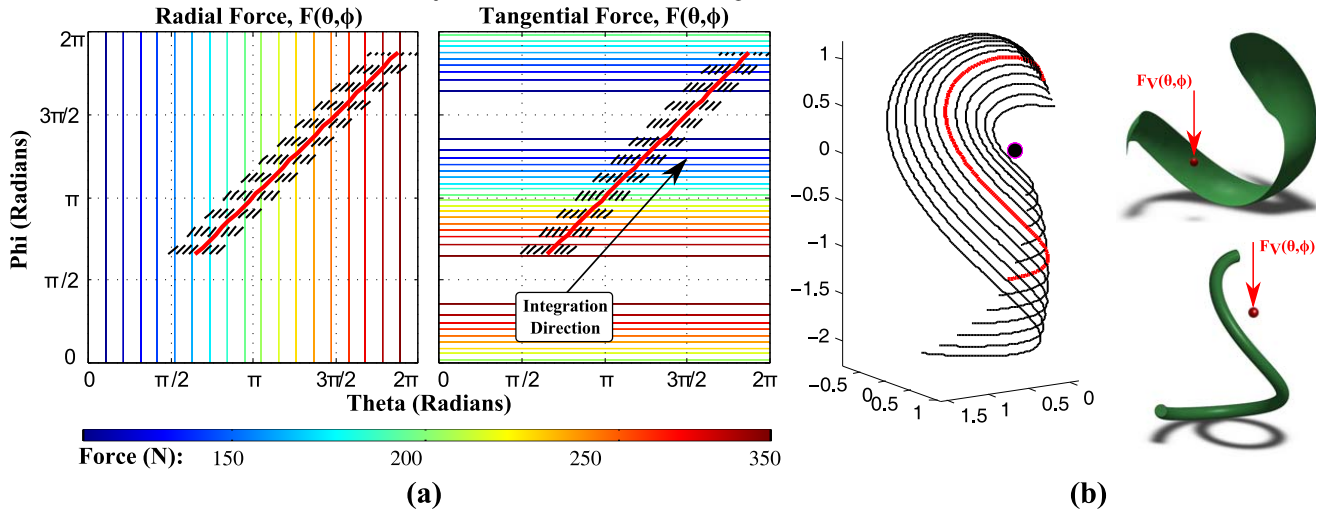
Fig. 11. **(a)** Radial and tangential ground reaction force definition of 3D KS. **(b)** Derived 3D surface and 3D curve KS, where the curve is the surface center.

5.3 Gait Correction and Prosthetics Shoe Soles

5.3.1 Shoe Sole Design

Shoe sole design impacts ground reaction force magnitude and direction during walking. These ground reaction forces can affect lower limb joints and muscles and/or the spine. A 3D KS can be derived that utilizes gait forces to mechanically filter and redirect these forces in order to change foot pressure distribution or foot orientation to alleviate walking problems.

Foot prosthesis design can greatly benefit from a 2D or 3D KS in order to predict foot roll over shape (ROS) kinetics during walking. Better ROS can result in more symmetric gait and less frictional forces at the stump.
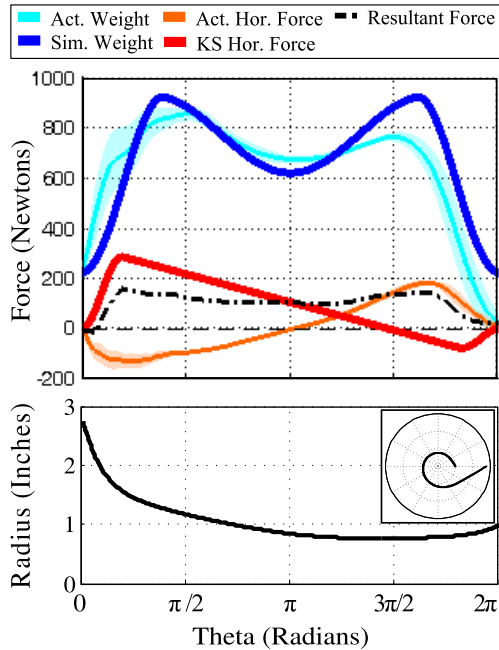

Fig. 12. A kinetic shape derived to react with a constant 100 N radial force when non-constant walking weight is applied.

5.3.2 GEMS Optimization Example

The Gait Enhancing Mobile Shoe (GEMS) [4, 5] is a novel device developed for lower limb rehabilitation, specifically asymmetric gait. The GEMS mimics a split-belt treadmill, which imposes different velocities on each tread, that is used in gait rehabilitation. However, the GEMS does not use any actuators or motors, but relies on passive spiral shaped wheels where the user's weight is transferred into a backward motion. The GEMS regulates the generated horizontal force from the spiral wheels using dampers and springs to create a safe overground velocity.

Human gait is divided into two phases: stance and swing. The stance phase consists of initial heel strike, mid-stance, and toe-off. During all three sub-phases the radial ground reaction forces vary from resistive forces at heel strike to assistive forces at toe-off, switching at mid-stance. Treadmills generate a constant backward velocity and the GEMS was initially designed to create a similar profile. However, the GEMS also affords the optimization of the velocity profile that includes non-constant velocities and force profiles. The KS wheel can be designed using the known applied weight during the stance phase so that the resulting horizontal force is any arbitrary profile desired.

Using actual kinetic gait data which was obtained by a person walking over a force plate multiple times, we derived a KS to produce a constant horizontal (radial) backward force of 100 N. The applied weight and horizontal (radial) reaction force trends were simulated as shown in Fig. 12. The simulated force definition used to derive the KS was

$$F_v(\theta) = 120\sin(1.5\theta) + 550\,\text{N} \qquad (31)$$
$$F_r(\theta) = (-71\theta + 228) + 100\,\text{N} \qquad (32)$$

To mimic actual data, the applied weight and desired horizontal force functions were windowed with a tapered Tukey window at a taper ratio of 0.4. The derived shape is shown in Fig. 12 with an initial radius of 2.78 in (7.00 cm). The resulting GEMS wheel shape will theoretically produce a constant backward force of 100 N. Given the derived wheel shape, the generated radial force is only dependent

on the applied weight. Therefore, it is irrelevant how many wheels the GEMS has since the applied weight is distributed through the number of wheels, hence producing a cumulative backwards force of 100 N.

6 Conclusion

We derived 2D and 3D formulas to produce KS defined by ground reaction forces when a known weight is applied. Three 2D shapes were tested statically and results were in good correlation with predicted values. During physical verification of 2D KS, it was found that a larger KS and KS with greater radial change produced more accurate readings. This can be accounted to surface finish and a more defined radius change. A dynamic analysis of the 2D shape showed the viability of using the 2D shape in dynamic applications such as plate dispensing and self-stabilization. A 3D KS that produces a radial and tangential force was defined and rendered, however, no static or dynamic physical verification was performed. Similar static and dynamic behaviors are expected in the radial and tangential directions. While much of current KS is presented in this paper, much is left to exploration and application of KS such as the physical verification of 3D KS, formal definition of dynamic KS behavior, and development of the proposed applications.

7 Acknowledgments

References

[1] Archimedes, 225 B.C.. *On Spirals*.

[2] Sakata, H., and Okunda, M. Fluid compressing device having coaxial spiral members. US patent 5,603,614, Sep. 30, 1994.

[3] Gilchrist, J., Campbell, J., Donnelly, C., Peeler, J., and Delaney, J., 1973. "Spiral plate method for bacterial determination". *American Society for Microbiology,* **25**(2), Feb, pp. 244–252.

[4] Handžić, I., Barno, E., Vasudevan, E. V., and Reed, K. B., 2011. "Design and pilot study of a gait enhancing mobile shoe". *J. of Behavioral Robotics,* **2**(4), pp. 193–201.

[5] Handžić, I., and Reed, K. B., 2011. "Motion controlled gait enhancing mobile shoe for rehabilitation". In Proc. IEEE Int. Conf. Rehabilitation Robotics, pp. 583–588.

[6] Sugiyama, Y., and Hirai, S., 2006. "Crawling and jumping by a deformable robot". *International Journal of Robotics Research,* **25**(5-6), Jun, pp. 603–620.

[7] Jardine, R. "Climbing Aids". US Patent 4,184,657, Jan. 22, 1980.

[8] Chen, F. Y., 1982. *Mechanics and design of cam mechanisms*, 18 ed. New York : Pergamon Press.

[9] Figliolini, G., Rea, P., and Angeles, J., 2006. "The pure-rolling cam-equivalent of the geneva mechanism". *Mechanism and Machine Theory,* **41**, pp. 1320–1335.

[10] Shigley, J. E., 2008. *Shigley's Mechanical Engineering Design*, Vol. 8. McGraw-Hill.

[11] Radzevich, S. P., 2012. *Dudley's Handbook of Practical Gear Design and Manufacture*. CRC Press.

[12] Zheng, E., Jia, F., Sha, H., and Wang, S., 2012. "Non-circular belt transmission design of mechanical press". *Mechanism and Machine Theory,* **57**, pp. 126–138.

[13] Ottaviano, E., Mundo, D., Danieli, G. A., and Ceccarelli, M., 2008. "Numerical and experimental analysis of non-circular gears and cam-follower systems as function generators". *Mechanism and Machine Theory,* **43**, pp. 996–1008.

[14] de Groot, A., Decker, R., and Reed, K. B., 2009. "Gait enhancing mobile shoe (GEMS) for rehabilitation". In Proc. Joint Eurohaptics Conf. and Symp. on Haptic Interfaces for Virtual Environment and Teleoperator Systems, pp. 190–195.

[15] Hall, L., and Wagon, S., 1992. "Roads and wheels". *Mathematics Magazine,* **65**(5), Dec, pp. 283–301.

[16] Bloom, J., and Whitt, L., 1981. "The geometry of rolling curves". *The American Mathematical Monthly,* **88**(6), Jun-Jul, pp. 420–426.

[17] Menant, J. C., Steele, J. R., Menz, H. B., Munro, B. J., and Lord, S. R., 2009. "Effects of walking surfaces and footwear on temporo-spatial gait parameters in young and older people". *Gait and Posture,* **29**, pp. 392–397.

[18] Hansen, A., Childress, D., and Knox, E., 2000. "Prosthetic foot roll-over shapes with implications for alignment of trans-tibial prostheses". *Prosthetics and Orthotics International,* **24**(3), pp. 205–215.

[19] Curtze, C., Hof, A. L., van Keeken, H. G., Halbertsma, J. P., Postema, K., and Otten, B., 2009. "Comparative roll-over analysis of prosthetic feet". *Journal of Biomechanics,* **42**(11), pp. 1746 – 1753.

[20] Hansen, A., and Wang, C., 2010. "Effective rocker shapes used by able-bodied persons for walking and fore-aft swaying: Implications for design of ankle-foot prostheses". *Gait and Posture,* **32**, pp. 181–184.

[21] Rietman, J., Postema, K., and Geertzen, J., 2002. "Gait analysis in prosthetics: Opinions, ideas and conclusions". *Prosthetics and Orthotics International,* **61**(1), pp. 50–57.

[22] Rodriguez, G., and Aruin, A., 2002. "The effect of shoe wedges and lifts on symmetry of stance and weight bearing in hemiparetic individuals". *Archives physical medicine & rehabilitation,* **83**(4), pp. 478–482.

[23] Landry, S., Nigg, B., and Tecante, K., 2010. "Standing in an unstable shoe increases postural sway and muscle activity of selected smaller extrinsic foot muscles.". *Gait and Posture,* **32**, Jun, pp. 215–9.

[24] Handžić, I., and Reed, K. B., 2013. "Validation of a passive dynamic walker model for human gait analysis". In Proc. IEEE Eng. Med. Biol. Soc.

[25] McGeer, T., 1990. "Passive Dynamic Walking". *Int. J. of Robotics Research,* **9**(2), pp. 62–82.

[26] Adamczyk, P. G., Collins, S. H., and Kuo, A. D., 2006. "The advantages of a rolling foot in human walking". *The J. of Experimental Biology,* **209**, pp. 3953–3963.

[27] Yates, R. C., 1947. *A Handbook on Curves and Their Properties*. J.W. Edwards, US Military Acadamy.